Please fill in the name of the event you are preparing this manuscript for.	Middle East Oil, Gas and Geosciences Show
Please fill in your 6-digit SPE manuscript number.	SPE-213326-MS
Please fill in your manuscript title.	Fully Coupled Hydromechanical Approach for Flow in Fractured Rocks Using Darcy-Brinkman-Biot

Please fill in your author name(s) and company affiliation.

Given Name	Surname	Company
Xupeng	He	King Abdullah University of Science and Technology
Zhen	Zhang	King Abdullah University of Science and Technology
Marwa	AlSinan	Saudi Aramco
Hyung	Kwak	Saudi Aramco
Hussein	Hoteit	King Abdullah University of Science and Technology

Abstract

Coupling flow with geomechanical processes at the pore scale in fractured rocks is essential in understanding the macroscopic fluid flow processes of interest, such as geothermal energy extraction, CO_2 sequestration, and hydrocarbon production from naturally and hydraulically fractured reservoirs. To investigate the microscopic (pore-scale) phenomena, we present a fully coupled mathematical formulation of fluid flow and geomechanical deformation to model the fluid flow in fractured rocks. In this work, we employ a Darcy-Brinkman-Biot approach to describe the fully coupled flow and geomechanical processes in fractured rocks at the pore scale. Darcy-Brinkman-Stokes (DBS) model is used to model multi-scale flow in the fractured rocks, in which fracture flow is described by Navier-Stokes equations and flow in the surrounding matrix is modeled by Darcy's law. With this approach, a unified conservation equation for flow in both media (fracture and matrix) is applied. We then apply Biot's poroelasticity theory and Terzaghi's effective stress theory to capture the geomechanical deformation. The continuity of the fluid pressure is imposed to connect the DBS equation and the stress-seepage equation. This coupled model is employed to determine the permeability within the microfracture. Numerical results show that this coupled approach can capture the permeability under the effects of solid deformation and multi-scale formation. We develop a fully coupled model to capture the pore-scale flow-geomechanically process in fractured rocks. To our knowledge, the fully coupled framework is developed and applied to characterize fracture permeability at the pore scale in fractured rocks for the first time.

Keywords: Darcy-Brinkman-Biot, fractured reservoirs, dual permeability, poroelasticity.

1. Introduction

Modeling fluid flow in subsurface fractured rocks is essential in various applications (Zhang et al., 2022a), such as geothermal extraction, CO_2 sequestration (Zhang et al., 2022b), and shale gas operation. Understanding the flow behavior in fractured rocks requires a proper way to describe the geo-mechanical behavior of the surrounding rocks (He et al., 2022b; Nelson, 2001).

Researchers have deployed the cubic law to describe the fluid flow with the assumption of two parallel and smooth plates for decades due to its efficiency. However, the rock surface tends to behave with strong roughness, significantly affecting the fractured rocks' flow behavior and corresponding physical properties (He et al., 2021a). Various modification has been proposed to improve the cubic law. Brown (1987) used the arithmetic mean to represent the aperture of the fracture, Smith and Freeze (1979) introduced the geometric mean of the aperture of the fracture, Zimmerman et al. (1991) proposed a correction factor to represent the effects of the roughness within fractures, and He et al. (2021a) introduced a corrected cubic law to account for the effects of the tortuosity and roughness. However, the influence of the geo-mechanical is not considered in the above-mentioned models. Chen et al. (2015) investigated the effects of effective stress on the permeability of shale gas reservoirs. Li et al. (2013) studied the stress sensitivity of porous rocks and fractures. Zhou et al. (2019) investigated the performance of the permeability change within a single fracture under highly effective stress. Wang et al. (2020) studied the hydraulic properties of rough-walled fractures under different shearing stresses. He et al. (2020) studied the hydraulic responses of the fractures under effective stresses. He et al. (2021b) investigated the influence of the normal and shear stress on the permeability change within fractures. However, the above-mentioned analytical methods suffer from strong assumptions and only work for specific cases.

To address this problem, researchers proposed high-resolution simulations using Navier-Stokes (NS) equations to describe the fluid flow within fractures. However, the porous media has multiscale features, which makes it infeasible to apply the NS equation everywhere. The rock often contains multi-scale features (Zhang et al., 2022c), and it is possible to introduce a threshold length to characterize two domains. Specifically, the porous domain is modeled using Darcy’s law, and the free channel is modeled using the NS equation. Therefore, researchers have started to utilize the micro-continuum approach to model fluid flow on both large scale and small scales. For instance, Soulaine and Tchelepi (2016) utilized the Darcy-Brinkman-Stokes to model the fluid flow in both the fracture and porous media using one unified governing equation. He et al. (2022a) utilized the extended Darcy-Brinkman-Stokes equation to describe the fluid flow within fractures using the Navier-Stokes equation and Darcy's law to describe the fluid flow within the surrounding matrix. He et al. (2021c) used the extended Darcy-Brinkman-Stokes equation to model the fluid leakage between the fractures and matrix.

Knowledge of how fluid flows in multiscale porous media is well established using the Darcy-Brinkman-Stokes equation. However, it is still challenging to describe the fluid flow in deformable porous media, meaning that the fluid can push the deformable rock when they flow through the channel, and in turn, the deformable rock can push back the fluid when they receive the force. We introduce the Darcy-Brinkman-Biot approach to model this phenomenon to capture complex physics, including the multiscale feature and the deformable porous media.

In this work, we introduced a method that can capture the multiscale and deformable features of the porous media to model the fluid flow within fractures. The outline of this paper is as follows: we first present the method in section 2 and then introduce the simulation model in section 3. The results are presented in section 4, and we present the conclusion in section 5.

2. Method

2.1 Darcy-Brinkman-Biot Method

Governing equation for the fluid phase

We start with the derivation of the mass and momentum conservation equations for the fluid, and we use $\mathbf{V_f}$ as the fluid velocity, ρ_f as the fluid density, P_f as the fluid pressure, and $\boldsymbol{\tau}_\mathbf{f}$ as the stress tensor:

$$\frac{\partial \rho_f}{\partial t} + \nabla \cdot (\rho_f \mathbf{V_f}) = 0 \tag{1}$$

$$\frac{\partial (\rho_f \mathbf{V_f})}{\partial t} + \nabla \cdot (\rho_f \mathbf{V_f} \mathbf{V_f}) = -\nabla P_f + \nabla \cdot \boldsymbol{\tau}_\mathbf{f}, \tag{2}$$

Then we upscale the Eq. (1) and Eq. (2) using volume averaging approach, which we can model multi-phase in a certain volume. We need to define an appropriate volume that is larger than any sub-volume of each phase to enable the averaging process when we use the volume averaging approach. Here we define two types of volume averaging, the intrinsic phase average A_i and superficial phase average $\overline{A_i}$. The intrinsic average A_i means the average properties of phase i over the volume of phase i, and superficial phase average $\overline{A_i}$ means the average properties of phase i over the entire defined volume, or the representative elementary volume (REV).

$$A_i = \frac{1}{V_i} \int_{V_i} A_i dV, \tag{3}$$

$$\overline{A_i} = \frac{1}{V_{REV}} \int_{V_{REV}} A_i dV = \phi_i A_i. \tag{4}$$

$$\phi_i = \frac{V_i}{V_{REV}} \tag{5}$$

The volume averaging method is used under the conditions that no mass transfer between solid and fluid phase, no chemical reaction, no slip effect at the interface between the solid and fluid phase, and the turbulence effects are neglectable. The the Eq. (1) and Eq. (2) becomes,

$$\frac{\partial (\rho_f \phi_f)}{\partial t} + \nabla \cdot (\rho_f \overline{\mathbf{V_f}}) = 0 \tag{6}$$

$$\frac{\partial (\rho_f \overline{\mathbf{V_f}})}{\partial t} + \nabla \cdot (\frac{\rho_f}{\phi_f} \overline{\mathbf{V_f}}\,\overline{\mathbf{V_f}}) = -\phi_f \nabla P_f + \nabla \cdot \overline{\boldsymbol{\tau}_\mathbf{f}} + \overline{\mathbf{F_f}} \tag{7}$$

Where the $\overline{\mathbf{F_f}}$ is the drag term between the solid and fluid phase that approach to 0 when ϕ_f close to 1. The stress tensor $\nabla \cdot \overline{\boldsymbol{\tau}_\mathbf{f}}$ can be expressed as,

$$\nabla \cdot \overline{\boldsymbol{\tau}_\mathbf{f}} = \nabla \cdot (\mu_f \nabla \overline{\mathbf{V}_\mathbf{f}} + \mu_f (\nabla \overline{\mathbf{V}_\mathbf{f}})^T) \tag{8}$$

We will use the Ergun equation to model the drag term between the fluid and solid phase, and we use k to represent the permeability in the REV scale. The permeability k is a function of the porosity ϕ_f, and k tends to become infinity when the ϕ_f approaches 1. The drag term $\overline{\mathbf{F_f}}$ can be expressed as,

$$\overline{\mathbf{F_f}} = -\phi_f \frac{\mu_f}{k(\phi_f)} (\overline{\mathbf{V_f}} - \overline{\mathbf{V_s}}) - \frac{1.75\rho_f}{(150{\phi_f}^3 k(\phi_f))^{1/2}} (\overline{\mathbf{V_f}} - \overline{\mathbf{V_s}}) | \overline{\mathbf{V_f}} - \overline{\mathbf{V_s}} | \tag{9}$$

Where the solid velocity is expressed as $\overline{\mathbf{V_s}}$. Here we assume the Reynolds number is smaller than 1, and then we can neglect the second term, which represents the non-linear inertial effects of the porous media. We then plug the Eq. (8) and Eq. (9) into Eq. (7), and get the following equations,

$$\frac{\partial(\rho_f \overline{\mathbf{V_f}})}{\partial t} + \nabla \cdot (\frac{\rho_f}{\phi_f} \overline{\mathbf{V_f}}\,\overline{\mathbf{V_f}}) = -\phi_f \nabla P_f + \nabla \cdot (\mu_f \nabla \overline{\mathbf{V_f}} + \mu_f (\nabla \overline{\mathbf{V_f}})^T) - \phi_f \frac{\mu_f}{k(\phi_f)} (\overline{\mathbf{V_f}} - \overline{\mathbf{V_s}}) \tag{10}$$

Here we use the intrinsic average pressure for the fluid because it align with the experimentally measured pressure value (Carrillo & Bourg, 2019). We can model the fluid flow in two different length scales by combining with the porosity field. Specifically, the Eq. (10) can approximate the NS equation when ϕ_f approaches 1 and k becomes infinity.

$$\frac{\partial(\rho_f \overline{\mathbf{V_f}})}{\partial t} + \nabla \cdot (\rho_f \overline{\mathbf{V_f}}\,\overline{\mathbf{V_f}}) = -\nabla P_f + \nabla \cdot (\mu_f \nabla \overline{\mathbf{V_f}} + \mu_f (\nabla \overline{\mathbf{V_f}})^T) \tag{11}$$

Eq. (10) can also approximate the Darcy's law as $\phi_f \in (0,1)$ and k is small.

$$(\overline{\mathbf{V_f}} - \overline{\mathbf{V_s}}) = -\frac{\nabla P_f k(\phi_f)}{\mu_f} \tag{12}$$

Governing equation for the solid phase

We use the same averaging method to derive the governing equations for the solid phase as we did for the fluid phase. Here we use the $\mathbf{V}_s$ as the solid velocity, ρ_s as the solid density, $\boldsymbol{\tau}_\mathbf{s}$ as the stress tensor, $\overline{\mathbf{F_s}}$ as the drag term, and $\boldsymbol{\tau}_\mathbf{T}$ as the Terzaghi stress tensor. The mass and momentum conservation equations for the solid phase are expressed as,

$$\frac{\partial(\rho_s \phi_s)}{\partial t} + \nabla \cdot (\rho_s \phi_s \overline{\mathbf{V_s}}) = 0 \tag{13}$$

$$\frac{\partial(\rho_s \phi_s \mathbf{V_s})}{\partial t} + \nabla \cdot (\rho_s \phi_s \mathbf{V_s}\mathbf{V_s}) = \phi_s \nabla \cdot \boldsymbol{\tau}_\mathbf{T} + \phi_s \nabla \cdot \boldsymbol{\tau}_\mathbf{s} + \overline{\mathbf{F_s}} \tag{14}$$

The terms in the right-hand side represent the pressure term, stress term, and drag term. The pressure term is expressed using the Terzaghi stress tensor $\boldsymbol{\tau}_{\mathbf{T}}$, and it can be expressed as the function of the confining pressure $\boldsymbol{\sigma}_{\mathbf{c}}$, pore fluid pressure P_f, and the swelling pressure P_{swell}.

$$\boldsymbol{\tau}_{\mathbf{T}} = \boldsymbol{\sigma}_{\mathbf{c}} - P_f\mathbf{I} - P_{swell}\mathbf{I} \tag{15}$$

We can represent the stress tensor $\boldsymbol{\tau}_{\mathbf{s}}$ as,

$$\nabla \cdot \boldsymbol{\tau}_{\mathbf{s}} = \nabla \cdot (\mu_s^{eff} (\nabla \mathbf{V}_{\mathbf{s}} + (\nabla \mathbf{V}_{\mathbf{s}})^T - \frac{2}{3}\nabla \cdot (\mathbf{V}_{\mathbf{s}}\mathbf{I}))) \tag{16}$$

Where μ_s^{eff} is the effective solid viscosity, and $\overline{\mathbf{F}_{\mathbf{s}}} = \overline{\mathbf{F}_{\mathbf{f}}}$ based on the momentum conservation. Then we can get the momentum equation in a volume averaged form as,

$$\begin{aligned}\frac{\partial(\rho_s\phi_s\mathbf{V}_{\mathbf{s}})}{\partial t} + \nabla \cdot (\rho_s\phi_s\mathbf{V}_{\mathbf{s}}\mathbf{V}_{\mathbf{s}}) = \phi_s\nabla \cdot (\boldsymbol{\sigma}_{\mathbf{c}} - P_f\mathbf{I} - P_{swell}\mathbf{I}) + \phi_s\nabla \cdot (\mu_s^{eff} (\nabla \mathbf{V}_{\mathbf{s}} + (\nabla \mathbf{V}_{\mathbf{s}})^T \\ - \frac{2}{3}\nabla \cdot (\mathbf{V}_{\mathbf{s}}\mathbf{I}))) - \phi_f \frac{\mu_f}{k(\phi_f)}(\mathbf{V}_{\mathbf{s}} - \mathbf{V}_{\mathbf{f}})\end{aligned} \tag{17}$$

Here we neglect the non-linear term in the drag term as we did in the derivation of the fluid governing equations. We can express Eq. (17) in the following form when we deal with the isotropic linear elastic solid phase,

$$\frac{\partial^2(\rho_s\phi_s\mathbf{U}_{\mathbf{s}})}{\partial t} - \nabla \cdot (\mu_s\phi_s\nabla \mathbf{U}_{\mathbf{s}} + \mu_s\phi_s(\nabla \mathbf{U}_{\mathbf{s}})^T + \phi_s\lambda_s tr(\nabla \mathbf{U}_{\mathbf{s}})I) = \phi_s\nabla \cdot \boldsymbol{\tau}_{\mathbf{T}} + \overline{\mathbf{F}_{\mathbf{s}}} \tag{18}$$

Where $\mathbf{U}_{\mathbf{s}}$ is the displacement vector of the solid. The full derivation can be found in this paper (Carrillo & Bourg, 2019). Due to the conservation of momentum, the solid stress should be balanced with the fluid stress,

$$\nabla \cdot \overline{\boldsymbol{\sigma}_{\mathbf{s}}} = \nabla \cdot \overline{\boldsymbol{\sigma}_{\mathbf{f}}}^{transferred} = \phi_s\nabla \cdot \boldsymbol{\tau}_{\mathbf{T}} + \overline{\mathbf{F}_{\mathbf{s}}} \tag{19}$$

Where $\boldsymbol{\sigma}_{\mathbf{s}}$ and $\boldsymbol{\sigma}_{\mathbf{f}}$ represent the viscous stress tensor of the solid phase and the fluid phase, and the superscript indicates that not all the fluid stress will transfer into the solid phase.

3. Simulation model

Here in this work, we modified the simulation model used in Carrillo et al. (2020)'s paper. The model was originally used to demonstrate the effectiveness of the multiphase Darcy-Brinkman approach without considering the geo-mechanical effects, in which the fluid flow within the fracture is modeled using the Navier-Stokes equation, and the fluid flow within the porous media is modeled using Darcy's law. We further combine the geo-mechanical process in this model and compute the permeability of the fracture under single-phase conditions. Specifically, we inject water in a 90% water-saturated microfracture. The detailed parameters are provided in **Table 1**.

Table 1. The parameters of the simulation model.

Parameters	Base case
Injection rate, [m/s]	0.1

Fracture porosity	0.5
Porous porosity	0.001
Water viscosity, [m^2/s]	1×10^{-6}
Water density, [kg/m^3]	1000
Solid density, [kg/m^3]	2650
Outlet pressure, [Pa]	0

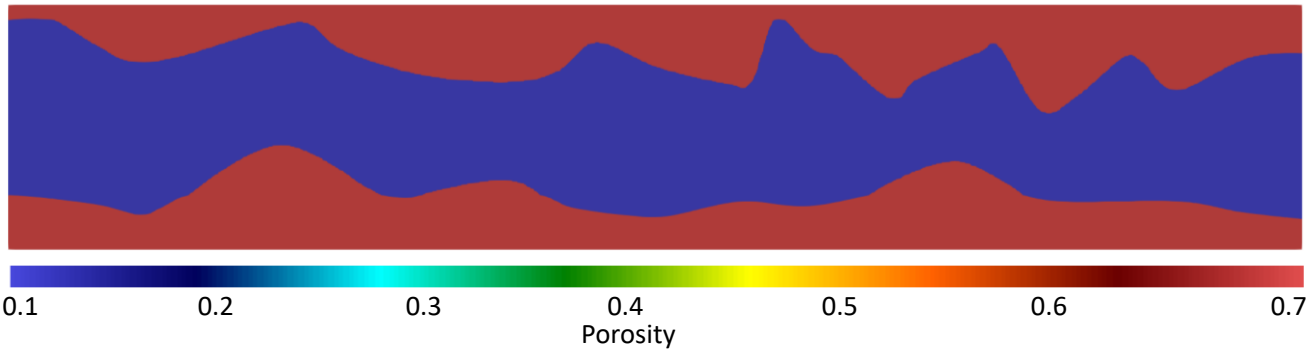

Figure 1. Porosity distribution in the microporous fracture, in which the blue color represents the fracture, and the red color represents the porous media.

Figure represents the porosity field of the microporous fracture. Specifically, the blue color represents the rough-walled fracture, and the red color represents the porous media. We then use the DBB approach to simultaneously model the single-phase flow at the fracture and porous media, in which Darcy's law is simulated within the porous media, and the Navier-Stokes equation is simulated within the fractures. We further combine the Biot equation to model the solid deformation under different pressures.

4. Results

The velocity field is shown in **Figure 2**, in which the black line represents the streamline of the fluid velocity. We can see that the fluid from the fracture can invade the matrix and vice versa. The velocity in the fracture is significantly larger than the matrix. We also notice that the low-velocity area within the fracture behind the roughed-wall area is indicated by the green color, which is reasonable because the roughed wall can reduce the fluid velocity. **Figure 3** shows the pressure distribution and the streamlines of the fluid velocity. We can see that the pressure difference drives the fluid flow.

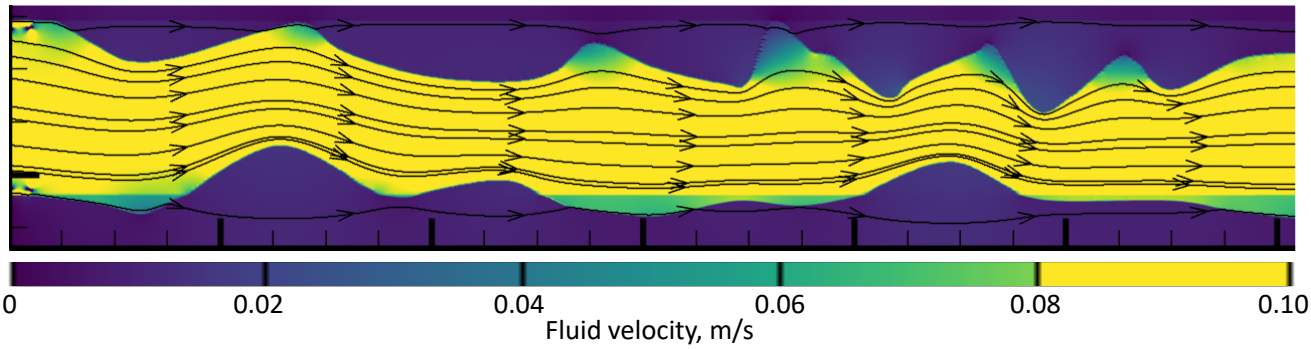

Figure 2. Fluid velocity distribution and fluid velocity streamlines in the microporous fracture.

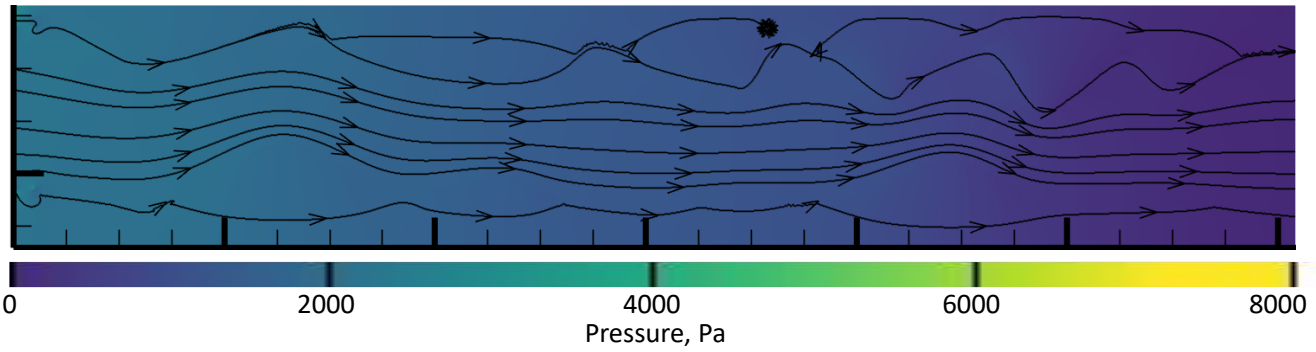

Figure 3. Fluid velocity streamlines and pressure distribution in the microporous fracture.

Figure 4 shows the solid velocity distribution. We can see that the solid velocity is much lower than the fluid velocity. The movement of the solid and fluid phases is modeled using Newton's Third Law. The fluid flow can push the solid phase, and as a result, the solid phase can push back the fluid. In this way, the model can capture the rock deformation effects. We can see that the high-velocity area of the solid phase is mainly located at the rough area, in which the fluid flow is blocked and the fluid exerts pressure on the solid phase.

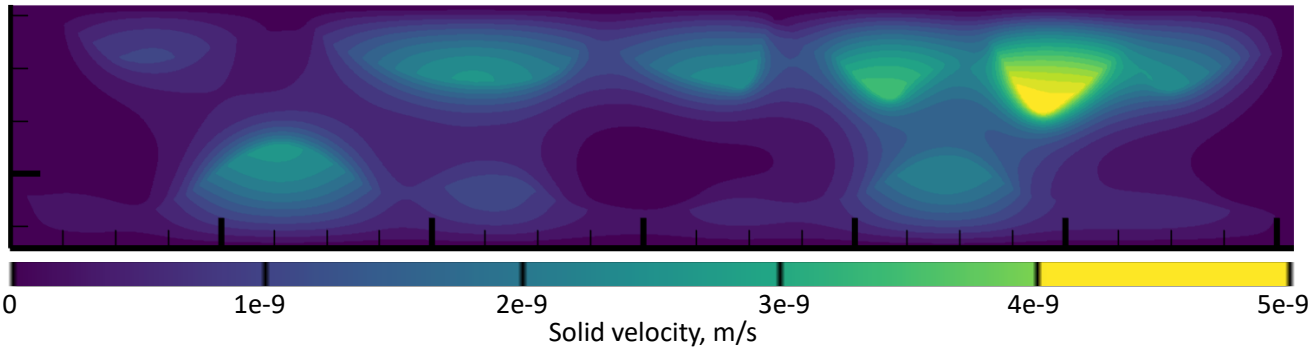

Figure 4. Solid velocity distribution in the microporous fracture.

We further compute the permeability of the microfracture formation using the Darcy's law as follows,

$$k = \frac{q\mu L}{A\Delta P} \tag{20}$$

The computed permeability is 6.14 Darcy. In this way, we can combine the effects of the solid movement on the permeability calculation.

5. Conclusions

This work presents a fully coupled model that can simultaneously model the fluid flow within two scales—specifically, the fracture and the porous media. Biot's theory is employed to capture the solid deformation effects. The Darcy-Brinkman-Stokes (DBS) model is used to model multi-scale flow in microfracture formation. The fluid flow within the fracture is modeled using the Navier-Stokes equation, and the fluid flow within the porous media is described using Darcy's law. We then employ this method to compute the permeability within a microfracture formation. Apparently, solid deformation can be observed by the solid velocity field. We further compute the permeability of the microfracture formation using Darcy's law. By doing this, we can consider the multi-scale fluid flow coupled with the geo-mechanical effects.

We present a fully coupled model to capture the flow-geomechanically process in fractured rocks. To our knowledge, the fully coupled geo-mechanical and multi-scale framework is developed and applied to characterize fracture permeability at the pore scale in fractured rocks for the first time.

References

Brown, S. R. (1987). Fluid flow through rock joints: the effect of surface roughness. *Journal of Geophysical Research: Solid Earth*, *92*(B2), 1337-1347.

Carrillo, F. J., & Bourg, I. C. (2019). A Darcy-Brinkman-Biot approach to modeling the hydrology and mechanics of porous media containing macropores and deformable microporous regions. *Water Resources Research*, *55*(10), 8096-8121.

Carrillo, F. J., Bourg, I. C., & Soulaine, C. (2020). Multiphase flow modeling in multiscale porous media: An open-source micro-continuum approach. *Journal of Computational Physics: X*, *8*, 100073.

Chen, D., Pan, Z., & Ye, Z. (2015). Dependence of gas shale fracture permeability on effective stress and reservoir pressure: model match and insights. *Fuel*, *139*, 383-392.

He, X., Alsinan, M., Kwak, H., & Hoteit, H. (2021c). High-Resolution Micro-Continuum Approach to Model Matrix-Fracture Interaction and Fluid Leakage. SPE Middle East Oil & Gas Show and Conference,

He, X., AlSinan, M., Zhang, Z., Kwak, H., & Hoteit, H. (2022a). Micro-continuum approach for modeling coupled flow and geomechanical processes in fractured rocks. SPE Annual Technical Conference and Exhibition,

He, X., Hoteit, H., AlSinan, M., & Kwak, H. (2020). Modeling hydraulic response of rock fractures under effective normal stress. ARMA/DGS/SEG International Geomechanics Symposium,

He, X., Santoso, R., Zhu, W., Hoteit, H., AlSinan, M., & Kwak, H. (2021b). Coupled Flow-Normal-Shear Influence on Fracture Permeability: Analysis and Modeling. ARMA/DGS/SEG 2nd International Geomechanics Symposium,

He, X., Sinan, M., Kwak, H., & Hoteit, H. (2021a). A corrected cubic law for single-phase laminar flow through rough-walled fractures. *Advances in Water resources*, *154*, 103984.

He, X., Zhang, Z., AlSinan, M., Li, Y., Kwak, H., & Hoteit, H. (2022b). Uncertainty and Sensitivity Analysis of Multi-Phase Flow in Fractured Rocks: A Pore-To-Field Scale Investigation. SPE Annual Technical Conference and Exhibition,

Li, S., Tang, D., Pan, Z., Xu, H., & Huang, W. (2013). Characterization of the stress sensitivity of pores for different rank coals by nuclear magnetic resonance. *Fuel*, *111*, 746-754.

Nelson, R. (2001). *Geologic analysis of naturally fractured reservoirs*. Elsevier.

Smith, L., & Freeze, R. A. (1979). Stochastic analysis of steady state groundwater flow in a bounded domain: 2. Two-dimensional simulations. *Water Resources Research*, *15*(6), 1543-1559.

Soulaine, C., & Tchelepi, H. A. (2016). Micro-continuum approach for pore-scale simulation of subsurface processes. *Transport in porous media*, *113*(3), 431-456.

Wang, C., Jiang, Y., Luan, H., & Sugimoto, S. (2020). Effect of shearing on hydraulic properties of rough-walled fractures under different boundary conditions. *Energy Science & Engineering*, *8*(3), 865-879.

Zhang, Z., He, X., AlSinan, M., Kwak, H., & Hoteit, H. (2022a). Robust Method for Reservoir Simulation History Matching Using Bayesian Inversion and Long-Short-Term Memory Network-Based Proxy. *SPE Journal*, 1-25. https://doi.org/10.2118/203976-pa

Zhang, Z., He, X., AlSinan, M., Li, Y., Kwak, H., & Hoteit, H. (2022b). Deep Learning Model for CO2 Leakage Detection Using Pressure Measurements. SPE Annual Technical Conference and Exhibition,

Zhang, Z., Li, Y., AlSinan, M., He, X., Kwak, H., & Hoteit, H. (2022c). Multiscale Carbonate Rock Reconstruction Using a Hybrid WGAN-GP and Super-Resolution. SPE Annual Technical Conference and Exhibition,

Zhou, J., Zhang, L., Li, X., & Pan, Z. (2019). Experimental and modeling study of the stress-dependent permeability of a single fracture in shale under high effective stress. *Fuel*, *257*, 116078.

Zimmerman, R., Kumar, S., & Bodvarsson, G. (1991). Lubrication theory analysis of the permeability of rough-walled fractures. International journal of rock mechanics and mining sciences & geomechanics abstracts,